

Disorder-induced resonance shifts in high-index-contrast photonic crystal nanocavities

L. Ramunno*

Department of Physics, University of Ottawa, Ottawa, Ontario, Canada K1N 6N5

S. Hughes†

Department of Physics, Queen's University, Kingston, Ontario, Canada K7L 3N6

(Received 11 December 2008; published 14 April 2009)

An optical scattering theory is introduced that predicts significant disorder-induced resonance shifts for photonic crystal nanocavities. These counterintuitive modal frequency shifts stem from the subtle role of local electric fields at perturbed (disordered) high-index-contrast interfaces. Using a representative cavity with a quality factor of 40 000 and an effective mode volume of $0.07 \mu\text{m}^3$, the cavity mode frequency is found to blueshift by up to several meV—even for nanometer-scale imperfections at the dielectric interface—which is several orders of magnitude larger than the cavity linewidth. These disorder-induced resonance shifts apply to a wide range of fabricated photonic nanostructures and scale approximately with the inverse mode volume.

DOI: 10.1103/PhysRevB.79.161303

PACS number(s): 42.70.Qs, 41.20.Jb, 42.25.Fx, 42.65.-k

Advanced lithography and etching techniques have recently led to major advances in the fabrication of nanoscale photonic crystals (PCs),^{1,2} whose functionalities are having a substantial impact on a broad range of scientific disciplines. Most notably has been the dramatic increase in the quality factor (Q) and decrease in effective mode volume (V_{eff}) of planar PC nanocavities.³ These large Q/V -ratio cavities are enabling the study of fundamentally new regimes of light-matter interaction, including single-exciton quantum electrodynamics,⁴ all-optical switching,⁵ and manipulation of dielectric particles.⁶ As these exciting applications emerge, understanding the complex light-matter interactions in sub-wavelength structures becomes very challenging, where new and unexpected physical effects can occur. In particular, fabricated artificial materials contain imperfections that lead to large scale disorder scattering, which can have severe consequences. For example, in the case of PC waveguides, so-called “lossless” slow-light modes exhibit major extrinsic scattering losses as the quasi-trapped light becomes increasingly sensitive to minute atomic-scale imperfections;^{7,8} for photonic metamaterials, even *arbitrarily small* amounts of material loss can make it impossible for nominally lossless waveguide modes to be stopped, and introduce impractically large propagation losses,⁹ acting to strongly perturb the nominal light-matter interactions and band structure.

The general optical theory of high-index photonic materials such as PCs typically involves solving Maxwell's electrodynamics equations over an ideal three-dimensional (3D) lattice with a spatially dependent dielectric constant.¹⁰ For complicated nanostructures, such approaches are problematic since an ideal structure is used to model the light-matter interactions, and thus it becomes difficult to account for unavoidable fabrication imperfections that may broaden and shift sharp features in the local density of photon states. While the importance of fabrication disorder on PCs is certainly becoming better established,¹¹ its effect on the properties of PC nanocavities—apart from a few qualitative studies on the overall effect on Q (Refs. 12 and 13)—remains unknown. In the meantime, it is now known that experiments on nominally identical samples vary from sample to

sample,¹⁴ which challenges our present understanding of the underlying physics.

In this Rapid Communication, we investigate the role of disorder-induced light scattering in high-index-contrast PC nanocavities (e.g., with $\epsilon=1$ and 12). We find an important and surprising result: there is a significant disorder-induced frequency shift of the cavity mode resonance even when the disorder function describing the imperfections has an ensemble average that is zero. Specifically, we predict a pronounced *blueshift* that can be traced back to the local-field perturbations in high-index-contrast structures. Yet, for low-index-contrast structures, no shift or a redshift is expected. The subtle role of local-field effects on frequency shifts of light scatterers has been pointed out in other contexts. For example, de Vries and Lagendijk¹⁵ studied resonant scattering and spontaneous emission in dielectrics with a microscopic derivation of local-field effects, with results that were generalized to disordered dielectrics. What is particularly surprising about our current findings is that even a 1-nm-scale disorder profile can have a considerable impact in well-confined cavity modes. Though we choose for our calculations a particular planar PC nanocavity using the popular $L3$ nanocavity³ [cf. Fig. 1(a)], our methods and general conclusions are applicable to arbitrary nanostructures, including

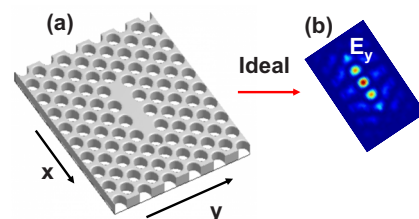


FIG. 1. (Color online) (a) Schematic of the planar PC that we study (Ref. 3). The nominal pitch is $a=420$ nm, except for two holes at the cavity edge that are shifted by $0.15a$; the slab thickness is $0.6a$. (b) A contour image of the calculated mode profile ($|E_y|^2$ at the slab middle) corresponding to the resonance frequency $\omega_h/(2\pi)=187$ THz; the quality factor is $Q\approx 40\,000$ and the effective mode volume is $V_{\text{eff}}=0.07 \mu\text{m}^3$.

nanostructured waveguides and photonic metamaterials.

Our formalism begins with the general eigenvalue equation for the electric field within an ideal (disorder-free) high-contrast nanostructure, $\nabla \times \nabla \times \mathbf{E}_h(\mathbf{r}) = \frac{\omega_h^2}{c^2} \varepsilon_p(\mathbf{r}) \mathbf{E}_h(\mathbf{r})$, where ε_p is the dielectric constant of the perfect structure, assumed to be real valued, and ω_h is the eigenvalue. The eigenmodes $\mathbf{E}_h(\mathbf{r})$ are quasitransverse and are the homogeneous solutions to the full eigenvalue equation of the true disordered system,

$$\nabla \times \nabla \times \mathbf{E}(\mathbf{r}) = \frac{\omega^2}{c^2} [\varepsilon_p(\mathbf{r}) + \varepsilon_{\text{dis}}(\mathbf{r})] \mathbf{E}(\mathbf{r}), \quad (1)$$

where $\varepsilon_{\text{dis}}(\mathbf{r})$ is the difference between the true and ideal dielectric constants, and thus characterizes the disorder. We seek the difference between the eigenvalues of the ideal and true descriptions, $\Delta\omega \equiv \omega - \omega_h$. By multiplying the ideal eigenvalue equation on the left by \mathbf{E}^* , and Eq. (1) on the left by \mathbf{E}_h^* , then integrating both over all space, we combine the resulting equations to obtain

$$\Delta\omega = -\frac{\omega_h}{2} \frac{\int \mathbf{E}_h^*(\mathbf{r}) \varepsilon_{\text{dis}}(\mathbf{r}) \mathbf{E}(\mathbf{r}) d\mathbf{r}}{\int \mathbf{E}_h^*(\mathbf{r}) [\varepsilon_p(\mathbf{r}) + \varepsilon_{\text{dis}}(\mathbf{r})] \mathbf{E}(\mathbf{r}) d\mathbf{r}}, \quad (2)$$

where we have assumed that $\Delta\omega \ll \omega_h$.

In standard low-index-contrast optical perturbation theories, one replaces \mathbf{E} by \mathbf{E}_h and assumes $\varepsilon_{\text{dis}} \ll \varepsilon_p$, giving $\Delta\omega_{\text{pert}} = -\frac{\omega_h}{2} \int \varepsilon_{\text{dis}}(\mathbf{r}) |\mathbf{E}_h(\mathbf{r})|^2 d\mathbf{r}$, where the normalization condition is taken to be $\int \varepsilon_p(\mathbf{r}) |\mathbf{E}_h(\mathbf{r})|^2 d\mathbf{r} = 1$. The statistics of $\Delta\omega_{\text{pert}}$ depends only on the ensemble average of ε_{dis} . As we show later, for planar nanostructures, this is not identically zero but it can result in zero-frequency shift if the field of the mode is parallel to the disordered interface(s). For high-index-contrast structures, one must go beyond perturbation theory as ε_{dis} can be large. This was discussed previously by Johnson *et al.*¹⁶ for anisotropically smoothed perturbations¹⁷ and for certain specific bump shapes and field components, showing that extra care is needed to take local-field effects into account. To do this, we define the Green's function, $\mathbf{G}(\mathbf{r}, \mathbf{r}')$ of the ideal system by $[\nabla \times \nabla \times - (\omega_h^2/c^2) \varepsilon_p(\mathbf{r})] \mathbf{G}(\mathbf{r}, \mathbf{r}') = (\omega_h^2/c^2) \delta(\mathbf{r} - \mathbf{r}') \mathbf{1}$, where $\mathbf{1}$ is the unit tensor. A rigorous solution to Eq. (1) is^{18,19}

$$\mathbf{E}(\mathbf{r}) = \mathbf{E}_h(\mathbf{r}) + \int_{-\delta V} \mathbf{G}(\mathbf{r}, \mathbf{r}') \mathbf{P}_{\text{eff}}(\mathbf{r}') d\mathbf{r}' - \mathbf{L} \frac{\mathbf{P}_{\text{eff}}(\mathbf{r})}{\varepsilon_p(\mathbf{r})}, \quad (3)$$

where $\mathbf{P}_{\text{eff}} = [\varepsilon_{\text{dis}} \omega^2 / \omega_h^2 - \varepsilon_p(\omega^2 / \omega_h^2 - 1)] \mathbf{E}$ is an effective scattering polarization. The integration volume is over all space but excludes an infinitesimal volume δV centered at $\mathbf{r} = \mathbf{r}'$, ensuring that the singularity of \mathbf{G} is excluded from the integral. The principal value of that singularity is contained in the last term, where \mathbf{L} is a constant depolarization tensor whose form depends weakly on the shape of δV (Ref. 19) and takes into account local fields. This can be understood more clearly if we consider the case of a small dielectric sphere with $\varepsilon = \varepsilon_2$ exposed to an external uniform field \mathbf{E}_h and surrounded by a homogeneous medium with $\varepsilon = \varepsilon_1$. Setting $\omega = \omega_h$ and taking the volume of that sphere to be δV ,

then $\mathbf{L} = (1/3) \mathbf{1}$ and the integral in Eq. (3) vanishes, giving a local field of $\mathbf{E} = 3\varepsilon_1 / [\varepsilon_2 + 2\varepsilon_1] \mathbf{E}_h$, as expected.²⁰

Our approach is to go one step beyond perturbation theory by using Eq. (3), which includes local-field corrections. Since we later use the finite-difference time-domain (FDTD) computational technique²¹ to find the unperturbed fields, we take δV as the size of a grid cell, which is justified as it is much smaller than a wavelength. Since this cell is then excluded from the integral in Eq. (3), and since the largest contributions to the real and imaginary parts of \mathbf{G} are near $\mathbf{r} = \mathbf{r}'$, we can neglect this integral to zeroth order. In general, the FDTD grid cell is a rectangular parallelepiped, and \mathbf{L} can be set according to the formula by Yaghjian.¹⁹ For brevity, we take the grid cell to be a cube, and thus set $\mathbf{L} = (1/3) \mathbf{1}$. The local field can then be approximated by $\mathbf{E}(\mathbf{r}) = 3\mathbf{E}_h(\mathbf{r}) / \{3 + [(\varepsilon_{\text{dis}}(\mathbf{r}) / \varepsilon_p(\mathbf{r}) - 1) \omega^2 / \omega_h^2 + 3]\}$. Since the volume of the disordered regions is much less than the effective mode volume of \mathbf{E}_h and $\Delta\omega \ll \omega_h$, we obtain from Eq. (2),

$$\Delta\omega = -\frac{\omega_h}{2} \int \varepsilon_{\text{dis}}^r(\mathbf{r}) |\mathbf{E}_h(\mathbf{r})|^2 d\mathbf{r}, \quad (4)$$

where $\varepsilon_{\text{dis}}^r(\mathbf{r}) \equiv 3\varepsilon_{\text{dis}}(\mathbf{r}) / [3 + \varepsilon_{\text{dis}}(\mathbf{r}) / \varepsilon_p(\mathbf{r})]$ is a “renormalized” disorder function that includes local-field effects.

It is interesting to note how Eq. (4) compares with the formula derived by Koenderink *et al.*²² for the frequency shift resulting from perturbation by a high-index atomic force microscope (AFM) probe. From their formula, we see that their frequency shift is (i) directly proportional to the unperturbed mode intensity, (ii) inversely proportional to the effective mode volume, and (iii) dependent on an effective polarizability, which in their case is a fixed parameter for the AFM probe tip. The scalings (i) and (ii) are essentially the same as in Eq. (4), taking into account our field mode normalization. Our formula, however, goes beyond (iii) by including the disorder-induced polarizability in each perturbation volume element around each disordered surface. In effect, we have nanometer-scale “local-field” probes that probe the induced polarizabilities and collectively sum them up to give the resonance shift, which is valid even in the absence of external perturbations.

While our disorder-induced frequency shift (4) is valid for arbitrary geometry, we consider in the remainder of this Rapid Communication patterned nanostructures within a slab. The ideal structure is thus defined by some pattern in the x - y plane that is vertically translated within the slab in the z direction. For many shapes, we can describe this patterning by an equation $f(x, y) = 0$, where the function f has units of length. In regions where $f > 0$ we set $\varepsilon = \varepsilon_1$, and in regions where $f < 0$ we set $\varepsilon = \varepsilon_2$. As examples, for a straight wall at $y = b$, $f = y - b$, and for a hole of radius R centered at the origin $f = \sqrt{x^2 + y^2} - R$. The ideal dielectric constant for z values within the slab is expressed in terms of f by $\varepsilon_p = \varepsilon_1 H(f) + \varepsilon_2 H(-f)$, where H is the Heaviside function. To describe surface roughness, we define T as the perpendicular distance between the sidewalls of the real and ideal structures; T is thus rapidly fluctuating in space. The disorder functions ε_{dis} and $\varepsilon_{\text{dis}}^r$ then take the explicit form

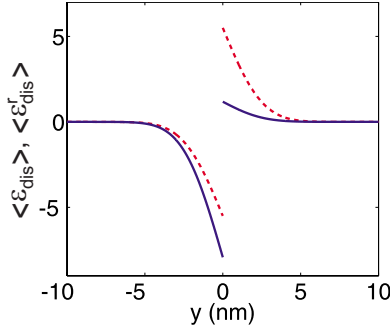


FIG. 2. (Color online) Plot of $\langle \epsilon_{\text{dis}} \rangle_{\text{ens}}$ (red dashed line) and $\langle \epsilon_{\text{dis}}^r \rangle_{\text{ens}}$ (blue solid line) within the slab versus y for a wall defined by $y=0$, where $\epsilon=12$ on the left, 1 on the right, and $\sigma=2$ nm.

$(\epsilon_2 - \epsilon_1)[A^{(r)}H(f)H(T-f) - B^{(r)}H(-f)H(f-T)]$, where $A=B=1$ for ϵ_{dis} , and $A^r=3\epsilon_1/(\epsilon_2+2\epsilon_1)$ and $B^r=3\epsilon_2/(\epsilon_1+2\epsilon_2)$ for ϵ_{dis}^r . For nanostructures created via lithography/etching, the roughness function T is reasonably well described by a Gaussian distribution, with a first-order probability function²³ $P_1(T) = \frac{1}{\sqrt{2\pi}\sigma} \exp(-\frac{T^2}{2\sigma^2})$, where σ is the characteristic rms roughness length, typically on the order of a few nanometers. Although $\langle T \rangle_{\text{ens}}=0$, $\langle \epsilon_{\text{dis}} \rangle_{\text{ens}}$, and $\langle \epsilon_{\text{dis}}^r \rangle_{\text{ens}}$ are not zero but are found to be

$$\langle \epsilon_{\text{dis}}^{(r)} \rangle_{\text{ens}} = \frac{(\epsilon_2 - \epsilon_1)}{2} \left[A^{(r)}H(f)\text{erfc}\left(\frac{f}{\sqrt{2}\sigma}\right) - B^{(r)}H(-f)\text{erfc}\left(\frac{-f}{\sqrt{2}\sigma}\right) \right], \quad (5)$$

where erfc is the complimentary error function. A plot of $\langle \epsilon_{\text{dis}} \rangle_{\text{ens}}$ and $\langle \epsilon_{\text{dis}}^r \rangle_{\text{ens}}$ for a straight sidewall at $y=0$ is shown in Fig. 2 versus distance from the sidewall, where $\epsilon=\epsilon_1=1$ for $y>0$ and $\epsilon=\epsilon_2=12$ for $y<0$.

The plot shows that $\langle \epsilon_{\text{dis}} \rangle_{\text{ens}}$ is antisymmetric across the sidewall. For low-index-contrast straight waveguides, this implies that there is no shift for field modes with \mathbf{E}_h parallel to the interface. This is because parallel components are continuous across the boundary, so that $\int \langle \epsilon_{\text{dis}} \rangle_{\text{ens}} |\mathbf{E}_h(\mathbf{r})|^2 d\mathbf{r}$ —and thus $\langle \Delta\omega_{\text{pert}} \rangle_{\text{ens}}$ —vanishes, assuming σ is small enough such that the mode is approximately uniform within a few σ of the boundary. However, field modes perpendicular to the interface do undergo a shift, since they are not continuous across the interface. The boundary conditions ensure that the small ϵ side always has the larger field value. Since this side also has positive $\langle \epsilon_{\text{dis}} \rangle_{\text{ens}}$ (cf. right side of Fig. 2), we find that $\langle \Delta\omega_{\text{pert}} \rangle_{\text{ens}} < 0$, indicating an expected redshift.

For high index contrast, however, we must use Eq. (4). As shown in Fig. 2 $\langle \epsilon_{\text{dis}}^r \rangle_{\text{ens}}$ is not antisymmetric but its absolute value is much larger on the high ϵ side (left). Hence, for high-index-contrast straight waveguides, field modes parallel to the interface do cause a shift, and from Eq. (4) we see that this results in $\langle \Delta\omega \rangle_{\text{ens}} > 0$, indicating an expected blueshift. For field modes with perpendicular components, the larger field side corresponds to the suppressed side of $\langle \epsilon_{\text{dis}}^r \rangle_{\text{ens}}$, which acts to suppress the expected redshift. Thus for arbitrary high-index-contrast structures, we expect (for most cases) an unavoidable overall blueshift, whereas for low-

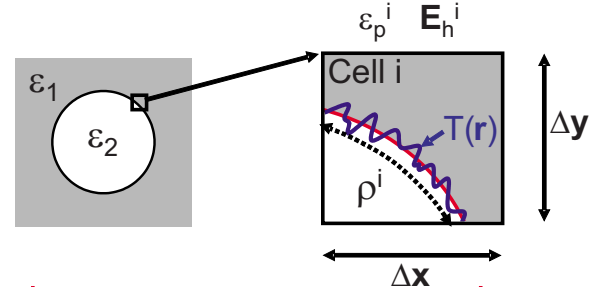


FIG. 3. (Color online) (Left) A top-view schematic of a single hole within a planar PC. (Right) Close up of a single grid cell, labeled by superscript “i.” The roughness function $T(\mathbf{r})$ is indicated by the blue line. The ideal structure boundary is indicated by the red line, whose length in cell i is ρ^i . The mean field and ideal dielectric constant within cell i are \mathbf{E}_h^i and ϵ_p^i , respectively.

index structures, we expect either no shift or a redshift.

To obtain the disorder-induced frequency shift quantitatively, we use FDTD to compute the mode \mathbf{E}_h . While this gives the field values at each grid cell, we also require a method of determining $\langle \epsilon_{\text{dis}}^r \rangle_{\text{ens}}$ at each grid cell. One such method is to analytically integrate the expression for $\langle \epsilon_{\text{dis}}^r \rangle_{\text{ens}}$ over a grid cell, but this is feasible only for straight waveguides. However, we can approximate this integral for arbitrary shapes through knowledge of the ideal dielectric constant within a grid cell, denoted by ϵ_p^i for cell i and the arclength of the ideal structure within the cell, ρ^i , as illustrated in Fig. 3; both quantities are easily obtainable. To approximate the spatial integral analytically, we first change coordinates from x and y to ones that are parallel and perpendicular to the wall. For the perpendicular coordinate, we take as the limits of integration the average distance on either side of the wall surface, thereby reducing the problem to a one-dimensional (1D) integral. We find these average distances to be $d_1^i = \Delta x \Delta y (\epsilon_p^i - \epsilon_1) / [\rho^i (\epsilon_2 - \epsilon_1)]$ for the ϵ_1 region and $d_2^i = \Delta x \Delta y (\epsilon_p^i - \epsilon_2) / [\rho^i (\epsilon_1 - \epsilon_2)]$ for the ϵ_2 region, where Δx and Δy are the grid cell lengths in x and y (cf. Fig. 3). Performing the integral, we obtain

$$\langle \epsilon_{\text{dis}}^r \rangle_{\text{ens}}^i = \frac{(\epsilon_2 - \epsilon_1) \rho^i}{\Delta x \Delta y} \left[\frac{3\epsilon_1 F(d_1^i)}{\epsilon_2 + 2\epsilon_1} - \frac{3\epsilon_2 F(d_2^i)}{\epsilon_1 + 2\epsilon_2} \right], \quad (6)$$

where $F(d) \equiv (1 - e^{-d^2/2\sigma^2})\sigma/\sqrt{2\pi} + \text{erfc}(d/\sqrt{2}\sigma)d/2$. Thus we derive a “user-friendly” discrete version of the disorder-induced frequency shift

$$\langle \Delta\omega \rangle_{\text{ens}}^i = -\frac{\omega_h}{2} \delta V \sum_i \langle \epsilon_{\text{dis}}^r \rangle_{\text{ens}}^i |\mathbf{E}_h^i|^2, \quad (7)$$

where \mathbf{E}_h^i is the numerically calculated field for cell i .

We now present quantitative numerical results for the planar PC cavity of Fig. 1. The dominant cavity mode profile within the center of the slab, which we calculated using FDTD,²¹ is shown in Fig. 1(b). The physics of the cavity mode is well established; light is trapped by the PC in the x and y directions, and bound by total internal reflection in the z direction. Coupling of the field mode to radiation modes above the light line causes decay of the field within the cav-

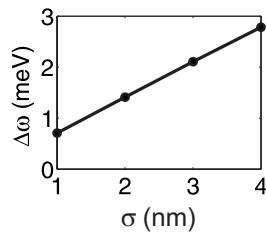


FIG. 4. Disorder-induced resonance shift versus σ for the cavity mode depicted in Fig. 1.

ity; this coupling is minimized by strategically moving two of the holes,³ resulting in a large Q and narrow linewidth $\Gamma = \omega_h/Q \sim 0.02$ meV. The disorder-induced frequency shift obtained via Eq. (7) is plotted in Fig. 4 as a function of σ . As expected from our previous discussion, we see an average blueshift of the cavity resonance. For typical state-of-the-art rms roughness lengths of $\sigma = 1\text{--}4$ nm, the resonance shift is calculated to be 1–3 meV, which is *several orders of magnitude larger than the nominal linewidth*. This evidently significant effect of disorder on the resonance peak is in contrast to previous qualitative discussions of disorder effects in PC cavities, where only the influence of disorder on the cavity Q (Refs. 12 and 13) was analyzed. Our results have important implications for all researchers exploiting these common nanocavities since designs based on a perfect (disorder-free) nanocavity will almost always incorrectly estimate the resonance peak and by a significant amount. Experimental veri-

fication of this effect would involve measuring the resonance shift as a function of one of the relevant parameters in the problem. One could, for example, measure an ensemble average of nominally identical samples, such as in Ref. 14, then compare the expected mean with different effective mode volume cavities. It is also important to note that around the mean resonance shift that we predict here, there will also be a fluctuation or variance in the frequency shift of an ensemble of nominally identical structures; the statistics of the latter will be important, e.g., in the context of coupled cavity resonators.²⁴

In conclusion, we have presented an optical scattering theory with supporting numerical calculations which predicts that PC nanocavities exhibit a significant disorder-induced frequency shift of the confined cavity mode. This manifests in a spectral blueshift of several meV—even with nanometer-scale fabrication imperfections—which, in our example, is two orders of magnitude larger than the nominal linewidth. Our general conclusions are not restricted to PC cavities and apply to a wide range of high-index-contrast photonic structures including PC waveguides, coupled cavities, and metamaterials.

This work was supported by the National Sciences and Engineering Research Council of Canada, the Canadian Foundation for Innovation, and the Canada Research Chairs program.

*lora.ramunno@uottawa.ca

†shughes@physics.queensu.ca

¹E. Yablonovitch, Phys. Rev. Lett. **58**, 2059 (1987).

²S. John, Phys. Rev. Lett. **58**, 2486 (1987).

³Y. Akahane, T. Asano, B. S. Song, and S. Noda, Nature (London) **425**, 944 (2003).

⁴T. Yoshie, A. Scherer, J. Hendrickson, G. Khitrova, H. M. Gibbs, G. Rupper, C. Ell, O. B. Shchekin, and D. G. Deppe, Nature (London) **432**, 200 (2004).

⁵See, e.g., M. Notomi, A. Shinya, S. Mitsugi, G. Kira, E. Kuramochi, and T. Tanabe, Opt. Express **13**, 2678 (2005).

⁶M. Barth and O. Benson, Appl. Phys. Lett. **89**, 253114 (2006).

⁷S. Hughes, L. Ramunno, J. F. Young, and J. E. Sipe, Phys. Rev. Lett. **94**, 033903 (2005).

⁸E. Kuramochi, M. Notomi, S. Hughes, A. Shinya, T. Watanabe, and L. Ramunno, Phys. Rev. B **72**, 161318(R) (2005).

⁹A. Reza, M. M. Dignam, and S. Hughes, Nature (London) **455**, E10 (2008).

¹⁰K. Sakoda, *Optical Properties of Photonic Crystals* (Springer, New York, 2005).

¹¹A. F. Koenderink, Ad Lagendijk, and W. L. Vos, Phys. Rev. B **72**, 153102 (2005).

¹²T. Asano, B.-S. Song, and S. Noda, Opt. Express **14**, 1996

(2006).

¹³D. Gerace and L. C. Andreani, Photonics Nanostruct. Fundam. Appl. **3**, 120 (2005).

¹⁴M. Barth, N. Nüsse, J. Sting, B. Löchel, and O. Benson, Appl. Phys. Lett. **93**, 021112 (2008).

¹⁵P. de Vries and Ad Lagendijk, Phys. Rev. Lett. **81**, 1381 (1998).

¹⁶S. G. Johnson, M. L. Povinelli, M. Soljačić, A. Karalis, S. Jacobs, J. D. Joannopoulos, Appl. Phys. B: Lasers Opt. **81**, 283 (2005).

¹⁷S. G. Johnson, M. Ibanescu, M. A. Skorobogatiy, O. Weisberg, J. D. Joannopoulos, and Y. Fink, Phys. Rev. E **65**, 066611 (2002).

¹⁸O. J. F. Martin and N. B. Piller, Phys. Rev. E **58**, 3909 (1998).

¹⁹A. D. Yaghjian, Proc. IEEE **68**, 248 (1980).

²⁰J. D. Jackson, *Classical Electrodynamics* (Wiley, New York, 1975), p. 151.

²¹We use FDTD Solutions by Lumerical Solutions Inc.

²²A. F. Koenderink, M. Kafesaki, B. C. Buchler, and V. Sandoghdar, Phys. Rev. Lett. **95**, 153904 (2005).

²³M. Skorobogatiy, G. Begin, and A. Talneau, Opt. Express **13**, 2487 (2005).

²⁴D. P. Fussell, S. Hughes, and M. M. Dignam, Phys. Rev. B **78**, 144201 (2008).